Pulsed precessional motion on the 'back of an envelope'

2003 J. Phys.: Condens. Matter 15 R1093

(http://iopscience.iop.org/0953-8984/15/24/203)

INSTITUTE OF PHYSICS PUBLISHING JOURNAL OF PHYSICS: CONDENSED MATTER

J. Phys.: Condens. Matter **15** (2003) R1093–R1100 PII: S0953-8984(03)33367-3

TOPICAL REVIEW

Pulsed precessional motion on the 'back of an envelope'

M Buess[1], Y Acremann[2], A Kashuba[3], C H Back[4] and D Pescia[1,5]

[1] Laboratorium für Festkörperphysik, Eidgenössische Technische Hochschule Zürich, CH-8093 Zürich, Switzerland
[2] Stanford Linear Accelerator Center 2575, Sand Hill Road, Mailstop 69 Menlo Park, CA 94025, USA
[3] L D Landau Institute for Theoretical Physics, 2 Kosygina street, 117334 Moscow, Russia
[4] Institut für Experimentelle und Angewandte Physik, Universität Regensburg, Universitätsstrasse 31, 93040 Regensburg, Germany

E-mail: pescia@solid.phys.ethz.ch

Received 3 December 2002
Published 6 June 2003
Online at stacks.iop.org/JPhysCM/15/R1093

Abstract

In a recent paper (Acremann *et al* 2000 *Science* **290** 492) the precessional trajectory of the magnetization vector was imaged with spatial resolution as a function of the time elapsed after a magnetic field pulse was applied. The most surprising observations—the reversal of the magnetic excitation upon reflection from the boundary and the spatial non-uniformities of the precessional mode—have remained unaccounted for so far. Here we present a 'back of the envelope' model of the precessional motion that is analytical, free of adjustable parameters, and that reproduces all the essential experimental features, including the behaviour of the dynamical magnetization at boundaries.

Let us consider applying a short magnetic field pulse to a magnetic element. If this field is not exactly parallel to the ground-state magnetization vector there will be a torque and the magnetization vector will start a *precessional motion*. This motion, which evolves typically on the picosecond timescale, can be imaged with spatial and time resolution [1–5]. The precessional mode might be technologically relevant; it has been suggested that it could become important for increasing data rates in magnetic recording [6]. In fact, it has recently been demonstrated that precessional switching with especially tailored magnetic field pulses can indeed be observed in microstructured magnetic elements [7, 8]. There are several fundamental questions on precessional motion that have not been answered satisfactorily so far. As the size of the magnetic structures which store the information is shrinking, the influence of the boundaries on the switching behaviour of the magnetic bits increases. Their role, however,

[5] Author to whom any correspondence should be addressed.

is, in our opinion, not well understood. A recent experiment, for instance, has provided images of the reflection of a spin excitation at the boundary of a micrometre-sized disc [2]. Surprisingly, the excitation was observed to reverse its sign upon reflection—a fact that has remained unexplained so far. A further key question for technological applications is whether the uniform precessional mode can be realized in micro- and nano-magnetic elements, so that switching can proceed in a controlled way. Several experiments [1, 2] reported a systematic development of spatial non-uniformities with unknown origin. Park *et al* reported two classes of excitations in systems with closure domain configurations localized within the domains and the domain walls. They also found edge localized modes that have previously been predicted from Brillouin light scattering experiments [4, 9]. On the other hand, a recent experiment [7] seems to have avoided those spatial non-uniformities by suitably shaping the magnetic element.

In this review, we provide an explanation for the observations reported in [2]. In that experimental work, the magnetic element was a very thin Co-disc (radius $R \sim 3\,\mu$m, thickness $d \sim 20$ nm), see figure 1(A). The ground-state magnetization distribution consisted of at least four in-plane magnetized domains (figure 1(B)) arranged to produce an almost 'circulating' flux-closure configuration (shown schematically in figure 1(C)). Of the experimental images taken after exciting the magnetization vector $\vec{M}$ with a short magnetic field pulse (see caption to figure 1(A)), we consider here the images pertaining to the component of the magnetization vector that could be detected with the greatest precision, namely the one perpendicular to the plane on the disc (M_z). The experimental signal of this component is about ten times stronger than the signal arising from the in-plane components. In [2], M_z was imaged as a function of the position within the disc and of the time t elapsed after application of the magnetic field pulse with $\approx 0.3\,\mu$m lateral spatial resolution and with picosecond time resolution. The images display—as expected from the symmetry of the ground state—an approximate axial symmetry, i.e. they are approximately invariant with respect to rotations around a z-axis passing through the centre of the disc (figure 1(D)). Because of this axial symmetry, we restrict ourselves, without losing experimental information, to re-plotting the experimental $M_z(t, \vec{r})$ of [2] along one single axis 'x' passing through the origin of the disc, see figure 2(top). In this figure, the spatial coordinate x is along the vertical scale, the time-coordinate t is along the horizontal scale. The grey scale used to plot the experimental data is a measure of the strength of M_z, white and black indicating opposite orientations. The main features of figure 2(top) are the following: the magnetic excitation builds up at the boundaries ('A'), propagates to the centre ('B'), where it is reflected back *with reversed amplitude*. After hitting the boundary of the disc, the excitation *reverses sign again* ('C') and travels back to the centre ('D'). The pattern of figure 2(top) can be roughly described as a $>$-shaped excitation repeating periodically in time. The period can be directly read out from the figure. The motion is non-uniform in space; in such a diagram a spatially uniform motion within the disc would appear as vertical stripes repeating in time. Notice that the contrast weakens as time elapses, this is due to energy dissipation which ultimately restores the ground-state in-plane magnetization.

We now proceed to construct a mathematical model of the experimental image (figure 2(top)). We assume that the local magnetization vector $\vec{M}(\vec{r}, t)$ obeys the Landau–Lifshitz (LL) equation (neglecting energy dissipating terms). In this equation, the torque on $\vec{M}$ is exerted by an effective magnetic field which includes the externally applied field pulse B_{ext}, the local exchange field B_{ex}, the effective fields arising from the various magnetic anisotropies of spin–orbit-coupling origin and the effective field originating from the dipolar interaction (from now on we will use $\vec{H}_{eff}$ because, by virtue of $\vec{B}_{eff} = H_{eff} + 4\pi\vec{M}$, it is the only component of $\vec{B}$ that actually exerts some torque on $\vec{M}$). Some aspects of figure 2(top) help us in weighting the role of the various effective magnetic fields in contributing to the motion of $\vec{M}$. The external magnetic field pulse triggers the motion; its time dependence

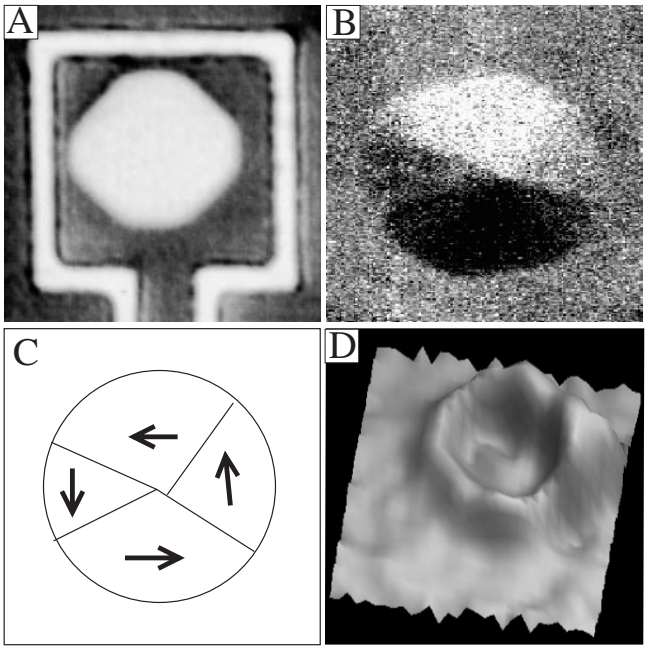

Figure 1. (A): optical micrograph of the Co-dot. The lateral size of the figure is 12 μm. The Co-dot is surrounded by a lithographically defined single-turn micro-coil into which a short current pulse is launched. The micro-coil is connected to a current source, which, in the experiments of [2] was an optically controlled, so-called Auston switch [2]. In an Auston switch device, a laser pulse (called the 'pump' pulse) is directed onto a GaAs crystal. The photo-generated carriers produce a current flowing between two contacts evaporated onto the crystal. Auston switches have rise times of a few picoseconds and decay times of the order of 100 ps [2]. The current pulse produces a magnetic field pulse perpendicular to the disc. (B): static domain distribution measured by scanning electron microscopy with polarization analysis (SEMPA). In SEMPA [2], the spin polarization of secondary emitted electrons is detected and is proportional to the surface magnetization within the electron beam focus. In this figure, the instrument is set to detect the in-plane component along the horizontal. The strong black–white contrast between the regions of the disc at the bottom and at the top is indicative of domains being magnetized parallel (antiparallel) to the horizontal direction. (C): schematic view of the static magnetization direction as obtained with SEMPA. (D): a three-dimensional plot of the M_z component at $\approx$200 ps after excitation, showing the axial symmetry. M_z was measured using the polar Kerr effect [10]. The laser beam, delayed by the time t with respect to the 'pump' laser pulse by an optical delay line, is directed perpendicularly onto the surface of the sample. Using a polarization sensitive detector, the polarization of the reflected light is detected. For symmetry reasons, the rotation of the polarization depends solely on the out-of-plane component of the magnetization. In our setup, we use a Wollaston prism which splits the reflected beam into its two polarization components. The intensity of the two components is measured using photodiodes. The difference of the two intensities is proportional to the Kerr rotation.

and strength are known approximately [2]. This field is applied perpendicularly to the film plane. Thus, it causes an initial in-plane deviation of $\vec{M}$ from its ground-state value that launches the time-dependent motion. This motion develops, as seen from the image, on spatial scales of the order of micrometres. On this scale, the order of magnitude of $(\gamma H_{ex})^{-1}$, which converts H_{ex} to the characteristic time it takes to see its effect on the precessional motion, is microseconds.This is because exchange fields are essentially proportional to the second derivative of the magnetization profile, and this is very small when the excitation occurs on micrometre spatial scales. Thus, we consider, from now on, the effective field arising from the

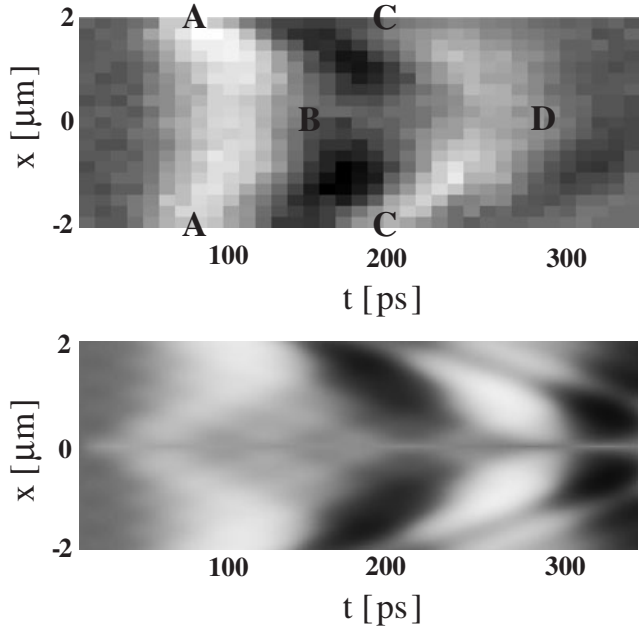

Figure 2. Top: the perpendicular component of the magnetization vector M_z is plotted using a grey scale along an axis x crossing the centre and at different times t after excitation by the external magnetic field pulse. Bottom: $M_z(x, t)$ calculated by superimposing 10 eigenmodes and using an external field pulse with 12 ps rise time and 150 ps decay time [2]. Notice that the picture obtained after superposition of the first six modes is essentially the same. As the field pulse has a finite band width and the higher modes have a smaller projection onto the quite uniform external field pulse, their contribution to the motion is negligible. To check for the accuracy of the variational eigenvalues, the eigenvalue problem was solved numerically within a trial space consisting of 15 basis functions.

exchange interaction as negligible on the timescale of figure 2(top). Notice that, within the timescale of figure 2(top), the exchange interaction produces a fine structure (such as a complex magnetization distribution at the centre of the disc) at spatial scales comparable to the so-called exchange length [11]. However, this spatial scale—typically some nanometres—is far below the spatial resolution of figure 2(top). For estimating the role of magnetic anisotropies, we consider the symmetry of the ground state. It is an in-plane flux-closure configuration that can be explained by the dipolar interaction alone without invoking magnetic anisotropies. We thus make the reasonable assumption that, besides the external applied magnetic pulse which starts the process, the leading contribution to the torque is provided by the dipolar field of magneto-static origin. The energy functional describing the total dipolar energy reads

$$\mathcal{E}_d[\vec{M}] = \frac{1}{2}\int\!\!\int \mathrm{d}^3\vec{r}\,\mathrm{d}^3\vec{s}\,\frac{\vec{\nabla}^r_{\parallel}\vec{M}_{\parallel}(\vec{r})\cdot\vec{\nabla}^s_{\parallel}\vec{M}^s_{\parallel}(\vec{s})}{|\vec{r}-\vec{s}|} + \int\!\!\int \mathrm{d}^3\vec{r}\,\mathrm{d}^3\vec{s}\,\frac{\partial_{z_r}M_z(\vec{r})\cdot\partial_{z_s}M_z(\vec{s})}{|\vec{r}-\vec{s}|} \tag{1}$$

where $\parallel$ indicates the vector components parallel to the plane where the disc resides and z is the coordinate perpendicular to it. This expression can be simplified using further elements of figure 2(top). Because of the circular symmetry of both the ground state and the dynamical M_z-mode, we introduce cylindrical coordinates $\vec{\rho} = (\rho, \varphi, z)$ to describe a point $\vec{r}$ and cylindrical unit vectors (e_ρ, e_φ, e_z) as basis vectors. We also estimate the deviation from the ground-state configuration to be smaller than 5% [2], so that the component of $\vec{M}$ along e_φ is assumed to remain equal to the ground-state value M_0^φ for all times. Thus, the functional derivative of

$\mathcal{E}_d[\vec{M}]$—which gives the effective field acting on $\vec{M}$—with respect to M_φ is set to zero and the corresponding terms in $\mathcal{E}_d[\vec{M}]$ are, to lowest order, neglected. We use the identity

$$\left(\partial_{z_r}\partial_{z_s} + \vec{\nabla}^r_\parallel \cdot \vec{\nabla}^s_\parallel\right)\frac{1}{|\vec{r}-\vec{s}|} = 4\pi\delta(\vec{r}-\vec{s}) \tag{2}$$

to write

$$\mathcal{E}_d[\vec{M}] \simeq 2\pi\,\mathrm{d}\int M_z^2(\rho)\,\mathrm{d}^2\vec{\rho} + \frac{\mathrm{d}^2}{2}\iint \nabla_\rho M^\rho(\rho)\frac{1}{|\vec{\rho}-\vec{\rho}'|}\nabla_{\rho'}M^{\rho'}(\rho')\,\mathrm{d}^2\vec{\rho}\,\mathrm{d}^2\vec{\rho}' \tag{3}$$

where $\nabla_\rho M_\rho \equiv \frac{1}{\rho}\frac{\partial}{\partial\rho}(\rho M^\rho(\rho))$. Equation (3) is a perturbative expression. The first term is the energy arising from the z-component of $\vec{M}$ appearing during the motion. It is of the order $d\cdot R^2$ and contributes an effective field of the order $d\cdot R^2/(d\cdot R^2)\approx 1$. The next term in M_z would contribute a field of the order d/R and is neglected because, as $d \ll R$, it would only provide a minor correction. Thus, the field acting onto $\vec{M}$ by virtue of the lowest-order term in M_z amounts to the standard 'demagnetizing' field $-4\pi M_z$ pointing in the direction opposite to M_z. This is the field of a perpendicularly magnetized plate with infinite radius. The finite radius introduces corrections of the order d/R which are neglected here. The second term is due to a radial component appearing during the motion. Its functional derivative is the radial field $H_\rho[M_\rho]$

$$H_\rho[M_\rho] = \mathrm{d}\frac{\partial}{\partial\rho}\int_{disc}\mathrm{d}^2\vec{\rho}'\,\frac{1}{|\vec{\rho}-\vec{\rho}'|}\frac{1}{\rho'}\frac{\partial}{\partial\rho'}(\rho' M_{\rho'}) \tag{4}$$

which is a linear functional of M_ρ. Notice that it is of the order d/R. However, if neglected, no precessional motion develops, in contrast to experiment. Thus, within this perturbational approach, it makes sense neglecting the contribution of order d/R to the effective field along z, but it makes no sense neglecting the contribution of the same order d/R to the radial field. Now that all relevant fields are specified, we can write down the LL equations for the three components of $\vec{M}$. In general, the LL equations couple the different components. By taking the second time derivative of M_ρ the LL equations can, in the present case, be decoupled to

$$\frac{\partial^2 M_\rho}{\partial t^2} = -\gamma M_0^\varphi\frac{\partial H_{ext}}{\partial t} + 4\pi\gamma^2(M_0^\varphi)^2 H_\rho[M_\rho] \tag{5}$$

$$M_z(t,\rho) = (4\pi\gamma M_0^\varphi)^{-1}\left[\sum_i \dot{c}_i(t)M_\rho^i(\rho) + \gamma M_0^\varphi H_{ext}(t,\vec{\rho})\right]. \tag{6}$$

Equation (5) shows explicitly that the problem cannot be reduced to a standard wave equation. Equation (6) allows M_z to be straightforwardly calculated once M_ρ is known. We seek a solution of equation (5) with the separation Ansatz $M_\rho(\rho,t) = \sum_i c_i(t)\cdot M_\rho^i(\rho)$. The radial functions $M_\rho^i(\rho)$ are the solutions of the eigenvalue equation[6] $H_\rho[M_\rho^i] = -N_\rho^i M_\rho^i$. Inserting the separation Ansatz in equation (5) leads to a set of decoupled ordinary differential equations for the coefficient c_i

$$\ddot{c}_i + \omega_i^2 c_i = -\gamma M_0^\varphi(H_{ext}(\rho), M_\rho^i(\rho))\dot{H}_{ext}(t) \tag{7}$$

where the eigenfrequencies ω_i are related to the sought for eigenvalues N_ρ^i by the relation $N_\rho \doteq 4\pi\cdot\omega^2/(4\pi\gamma M_0^\varphi)^2$. The external field pulse is written as $H_{ext}(t)\cdot H_{ext}(\rho)$. The dependences of both t and ρ are known approximately, see [2]. As equation (7) is the equation of motion of a classical undamped forced harmonic oscillator, it can be solved analytically:

$$c_i = -\gamma M_0^\varphi(H_{ext}(\rho), M_\rho^i(\rho))\int_{-\infty}^{\infty}\dot{H}_{ext}(\tau)G(t,\tau)\,\mathrm{d}\tau \tag{8}$$

[6] The eigenfunctions can be orthogonalized to $(M_\rho^i, M_\rho^j) = \delta_{ij}$ with respect to the scalar product $(a,b) = \int_0^R a(\rho)b(\rho)2\pi\rho\,\mathrm{d}\rho$.

with the Green function $G(t, \tau) = \frac{1}{\omega_i} \sin(\omega_i(t-\tau))$. One interesting particular case is provided by $H_{ext}(t) \propto \delta(t)$. This problem can be solved at a glance. Its solution is equivalent to an 'initial condition' problem where there is no applied field pulse but the motion is initiated by imposing a finite value to M_ρ at $t = 0$. This is the 'initial condition' scenario used to give a rough explanation of the motion in [2]. For a pulse with a more complicated shape, the time integral can be performed numerically. Roughly speaking, the amplitude c_i is related to the amplitude of the time Fourier transform of the external field pulse at the frequency ω_i.

The key elements of this problem are the eigenvalues N_ρ^i and the eigenmodes $M_\rho^i(\rho)$. Once they are specified the motion is completely known. To determine them we first notice that the integral in equation (4) diverges for $\rho = 0$ unless $M_\rho|_{\rho=0}$ is zero. This establishes the first boundary condition: the radial component of the magnetization must vanish in the centre of the disc. Next, we notice that the exact solution of the eigenvalue equation for a disc with infinite radius is $N_\rho = 2\pi d \cdot k_\rho$ and $M_\rho \propto J_1(k_\rho \rho)$, J_1 being the first-order Bessel function and k_ρ being the in-plane radial wavevector labelling the low energy excitations with frequency $\omega \propto \sqrt{k_\rho}$. When the disc has a finite radius, H_ρ^{op} contains a contribution arising from the 'magnetic charge' building up at $\rho = R$ by virtue of the abrupt change of M_ρ from $M_\rho(R)$ to zero. This contribution diverges unless $M_\rho(R) = 0$. This establishes the second boundary condition. Thus, within our two-dimensional model, the appearance, during the motion, of a finite radial component M_ρ at the centre of the disc or at the boundary $\rho = R$ is associated with an infinite magneto-static energy, so that pinning $M_\rho|_{0,R} = 0$ must be introduced to avoid this divergence. By virtue of the vanishing of M_ρ at $\rho = R$, the operator H_ρ^{op} defined on a disc with finite radius becomes an hermitic one. In the spirit of the Ritz variational principle, $J_1(k_\rho \rho)$ are 'good' eigenfunctions for finite R as well, provided k_ρ is chosen to fulfil the boundary condition $J_1(k_\rho \rho)|_{\rho=R} = 0$. This produces a discrete set of eigenvalues N_ρ^i and a complete orthonormal basis set M_ρ^i on the disc. The analytical mode expansion of $M_z(t, \rho)$, calculated using these eigenfunctions and eigenvalues, is plotted in figure 2(bottom). This figure, which essentially shows how the mixture of eigenmodes evolves in time and space, reproduces qualitatively as well as quantitatively the >-shaped excitation front. In particular, the back and forth propagation of the excitation crest between A, B, C, D is the result of eigenmodes with appropriate frequency and spatial dependence coherently superimposing to move the excitation crest and change its sign as observed in the experiment.

Notice that the theoretical pattern contains, in the very initial stages of the motion, sizable contrast in the inner regions of the disc. This contrast is due to a portion of the excitation developing from the middle of the disc. However, the pattern calculated in figure 2(bottom) assumes immediate penetration of the applied magnetic field pulse into the whole disc. The order of magnitude of the characteristic time that it takes a magnetic field to penetrate a metallic object is $\tau \sim 4\pi\sigma l^2/c^2$, where σ is the conductivity and l is a characteristic linear dimension of the conductor [12]. To decide whether the characteristic length l, for a disc, is its thickness (in which case the orthogonal component of the field would penetrate through the film surface) or its radius (penetration from the side), we solve the equation describing the field dynamics in an infinitely extended film: $(\nabla)^2 B_z = \frac{4\pi\sigma}{c^2} \frac{\partial B_z}{\partial t}$. The Ansatz is $B_{z,m} = \mathrm{e}^{-t/\tau_m} B_{z,m}(z)$ [12], where τ_m are the eigenvalues of the equation $\frac{\partial^2 B_{z,m}}{\partial z^2} = -\frac{4\pi\sigma}{\tau_m c^2} B_{z,m}$. Because of the boundary conditions, this equation has non-zero solutions only for discrete values of τ_m, the largest value determining the characteristic times of penetration or expulsion [12]. The general solution of the eigenvalue equation is

$$B_{z,m} = a_m \cos\sqrt{\frac{4\pi\sigma}{\tau_m c^2}} z + b_m \sin\sqrt{\frac{4\pi\sigma}{\tau_m c^2}} z. \tag{9}$$

For the model of an infinite sheet, $\mathrm{div}\,\boldsymbol{B} = \frac{\partial B_z}{\partial z} \equiv 0$. This leads to $\sqrt{\frac{4\pi\sigma}{\tau_m c^2}} = 0$ i.e. the only possible eigenvalue is $1/\tau_m = 0 \Longleftrightarrow \tau_m = \infty$. This means that, for a disc with finite radius, the sought for characteristic length is the radius of the disc and that the field penetration occurs from the side. Thus, we do not expect the portion of the excitation developing from the central part of the disc to be observed experimentally, i.e. we expect a better physical description if one removes the contrast in the inner region of figure 2(bottom) during the initial stages of motion. This is in agreement with the experimental image (figure 2(top)).

In summary, we have constructed a 'back of the envelope' solution of the LL equation of motion for the geometry and the experimental parameters used in the experiments of [2]. The solution, which contains reasonable approximations but does not contain adjustable parameters, essentially reproduces the experimental spatio-temporal evolution of the spin excitation in the disc. The most striking experimental observations—the reversal of the sign of the excitation upon reflection and the quenching of the spatially uniform mode of precession—are a direct consequence of the pinning of the magnetization at the centre and at the border of the disc. This pinning, which was introduced to avoid unphysical singularities in our model, needs a thorough discussion. Magnetic fields are, strictly speaking, only singular at boundaries in the two-dimensional limit which we have adopted here [13–15]. In reality, boundaries have a finite thickness and, although the fields might become large, they remain finite at two-dimensional surfaces [13]. In the present case, $H_\rho|_{z=0,\rho\to R^-} \to -2\pi M_\rho(R)$ [16]. Although we have neglected exchange fields, their contribution to the torque might become sizable at distances from the border comparable to the exchange length [14]. While the dipolar interaction opposes the appearance of a radial component of the magnetization at the border, the stiffness against misalignment introduced by the exchange interaction favours the appearance of such a component at the border if one is present within the disc. Thus, although the reversal of the sign of the excitation indicates that the magnetization at the border of the disc is pinned, we actually do not know exactly—neither experimentally nor theoretically—what happens to the magnetization vector at the border. In general, the boundary conditions become increasingly complicated when the exchange field becomes more relevant, which is the case for nanoscale magnetic elements or for higher modes in micron-scale elements, and magnetic anisotropies play a role [17]. Then, the boundary conditions depend on the length scale of the excitation. Thus, requiring pinning of the magnetization vector or setting its normal derivative at surfaces to zero [11] is only a practical way to reduce the amount of simulation work involved; the actual motion could be subject to more complicated boundary conditions. It will be one major task of future experiments with high spatial resolution, e.g. at advanced x-ray sources, to determine accurately the motion of spins close to boundaries, where, in our opinion, the main physics resides.

Acknowledgment

We acknowledge the financial help by an internal ETH-grant and by SNF.

References

[1] Hiebert W K, Stankiewicz A and Freeman M R 1997 *Phys. Rev. Lett.* **79** 1134
[2] Acremann Y *et al* 2000 *Science* **290** 492 and the references therein
Acremann Y 2001 *Diss. ETH Nr 14389* available on request
[3] Mathieu C *et al* 1998 *Phys. Rev. Lett.* **81** 3968
[4] Park J P, Eames P, Engebretson D M, Berezovsky J and Crowell P A 2002 *Phys. Rev. Lett.* **89** 277201
[5] Park J P, Eames P, Engebretson D M, Berezovsky J and Crowell P A 2003 *Phys. Rev.* B **67** 020403(R)

[6] Back C H *et al* 1999 *Science* **285** 864
[7] Gerrits Th *et al* 2002 *Nature* **418** 509
[8] Schumacher H W, Chapert C, Sousa R C, Freitas P P and Miltat J 2003 *Phys. Rev. Lett.* **90** 017204
[9] Jorzick *et al* 2002 *Phys. Rev. Lett.* **88** 047204
[10] Woike Th, Kerkmann D, Beier th, Krasser W and Pescia D 1991 Method of and apparatus for the reading of magnetically stored information *US Patent Specification Number* 5,016,992
[11] Miltat J, Albuquerque G and Thiaville A 2001 An introduction to micromagnetics in the dynamical regime *Spin Dynamics in Confined Magnetic Structures* ed B Hillebrands and K Ounadjela (Berlin: Springer)
[12] Landau L D and Lifshitz E M 1960 Electrodynamics of Continuous Media *Course of Theoretical Physics* vol 8 (Oxford: Pergamon) pp 186–9
[13] Jackson J D 1998 *Classical Electrodynamics* 3rd edn (New York: Wiley) pp 75–9
[14] Rawe W, Ramstöck K and Hubert A 1998 *J. Magn. Magn. Mater.* **183** 329
[15] Thiaville A, Tomas D and Miltat J 1998 *Phys. Status Solidi* **170** 125
[16] Guslienko K Yu and Slavin A N 2000 *J. Appl. Phys.* **87** 6337
[17] Labrune M and Miltat J 1995 *J. Magn. Magn. Mater.* **151** 231